Journal of Pathology
J Pathol October 2023; **261**: 184–197
Published online 11 August 2023 in Wiley Online Library
(wileyonlinelibrary.com) DOI: 10.1002/path.6162

ORIGINAL ARTICLE

Forward genetics and functional analysis highlight *Itga11* as a modulator of murine psoriasiform dermatitis

Katja Bieber[1,2*], Siegfried Bezdek[1,3], Yask Gupta[1,2], Artem Vorobyev[1,2], Tanya Sezin[1,3], Natalie Gross[1,2], Jasper Prüssmann[1,3], Jean-Paul Sayegh[1,3], Mareike Becker[1,3], Sadegh Mousavi[1,3], Ashref Hdnah[1,3], Sven Künzel[4], Saleh M Ibrahim[1,2,5], Ralf J Ludwig[1,2†], Donald Gullberg[6†] and Christian D Sadik[1,3†]

[1] *Center for Research on Inflammation of the Skin, University of Lübeck, Lübeck, Germany*
[2] *Lübeck Institute of Experimental Dermatology, University of Lübeck, Lübeck, Germany*
[3] *Department of Dermatology, Allergy, and Venereology, University of Lübeck, Lübeck, Germany*
[4] *Max-Planck Institute for Evolutionary Biology, Plön, Germany*
[5] *College of Medicine, Khalifa University, Abu Dhabi, United Arab Emirates*
[6] *University of Bergen, Bergen, Norway*

**Correspondence to: K Bieber, Lübeck Institute of Experimental Dermatology, University of Lübeck, Ratzeburger Allee 160, D-23538 Lübeck, Germany. E-mail: katja.bieber@uksh.de*

†Equal contributions.

Abstract

Psoriasis is a chronic inflammatory skin condition. Repeated epicutaneous application of Aldara® (imiquimod) cream results in psoriasiform dermatitis in mice. The Aldara®-induced psoriasiform dermatitis (AIPD) mouse model has been used to examine the pathogenesis of psoriasis. Here, we used a forward genetics approach in which we compared AIPD that developed in 13 different inbred mouse strains to identify genes and pathways that modulated disease severity. Among our primary results, we found that the severity of AIPD differed substantially between different strains of inbred mice and that these variations were associated with polymorphisms in *Itga11*. The *Itga11* gene encodes the integrin α11 subunit that heterodimerizes with the integrin β1 subunit to form integrin α11β1. Less information is available about the function of ITGA11 in skin inflammation; however, a role in the regulation of cutaneous wound healing, specifically the development of dermal fibrosis, has been described. Experiments performed with *Itga11* gene-deleted (*Itga11*$^{-/-}$) mice revealed that the integrin α11 subunit contributes substantially to the clinical phenotype as well as the histopathological and molecular findings associated with skin inflammation characteristic of AIPD. Although the skin transcriptomes of *Itga11*$^{-/-}$ and WT mice do not differ from one another under physiological conditions, distinct transcriptomes emerge in these strains in response to the induction of AIPD. Most of the differentially expressed genes contributed to extracellular matrix organization, immune system, and metabolism of lipids pathways. Consistent with these findings, we detected a reduced number of fibroblasts and inflammatory cells, including macrophages, T cells, and tissue-resident memory T cells in skin samples from *Itga11*$^{-/-}$ mice in response to AIPD induction. Collectively, our results reveal that *Itga11* plays a critical role in promoting skin inflammation in AIPD and thus might be targeted for the development of novel therapeutics for psoriasiform skin conditions.

Keywords: psoriasis; fibroblasts; ITGA11; Aldara-induced psoriasiform dermatitis model; skin inflammation; forward genetics; RNA-seq

Received 15 September 2022; Revised 7 June 2023; Accepted 13 June 2023

No conflicts of interest were declared.

Introduction

Psoriasis is a chronic inflammatory disease of the skin and joints that has been diagnosed in ~2–3% of the Western population [1] and includes both autoinflammatory and autoimmune features. While its pathogenesis is only partially understood, there is a broad consensus that genetic factors contribute significantly to this disorder. Accordingly, human genome-wide association studies (GWAS) have been instrumental in elucidating the pathways underlying disease pathology and have resulted in the identification of more than 80 susceptibility loci [2]. The products of some of these loci, for example, the interleukin-23 receptor (*IL23R*) and the nonreceptor tyrosine kinase *TYK2*, have both been identified as highly effective pharmacological targets for the treatment of psoriasis, confirming the validity of the GWAS results [3,4].

In recent years, research on psoriasis has also been advanced by the development of novel mouse models [5,6]. Among these models, the Aldara®-induced

psoriasiform dermatitis (AIPD), also known as 'imiquimod-induced psoriasiform dermatitis', has become the most widely used preclinical model of this disease. In this model, an immune response is induced in the skin by the repeated topical application of Aldara® cream (Meda Pharma, Stockholm, Sweden). While the toll-like receptor (TLR)7/8 agonist, imiquimod (IMQ) is the active ingredient in Aldara®, the vehicle contains a significant amount of isostearic acid that can activate the NLRP1 inflammasome in keratinocytes [7]; both IMQ and isostearic acid contribute to the induction of dermatitis in this model [7]. The AIPD model captures many of the key clinical, histopathological, and molecular features of human psoriasis, including keratinocyte hyperproliferation, dermal infiltration with T cells, monocytes/macrophages, and neutrophils, and dermal neoangiogenesis, as well as the central role of T cells and T-cell cytokines, including IL-17A, IL-23, tumor necrosis factor (TNF)-α, and type I interferons [8,9]. Given their similar cellular and molecular mechanisms, the AIPD model is a valuable preclinical tool for the study of human plaque psoriasis and the development of novel therapeutic strategies.

As part of the first description of the AIPD model, van der Fits *et al*. (2009) reported differences in clinical severity when comparing the responses of *BALB/c* and *C57BL/6* inbred strains of mice. Our group demonstrated that the course of AIPD also differed significantly in *C57BL/6J* compared to *C57BL/6N* mice [10]. Taken together, these results suggest that the responses leading to AIPD are strain-dependent. Strain dependency was further corroborated by Swindell *et al*. (2017), who evaluated the variable clinical severity of AIPD in six inbred strains (*C57BL/6J*, *MOLF/EiJ*, *FVB/NJ*, *129X1/SvJ*, *BALB/cJ*, and *DBA/1*) and one outbred (*CD1*) strain of mice. Among the results of this study, the authors reported that *C57BL/6J* and *MOLF/EiJ* mice developed severe AIPD, while *FVB/NJ* mice remained relatively protected. Furthermore, these differences were paralleled by distinct transcriptomic profiles identified in inflamed skin. As reported previously [6], the skin transcriptome of *C57Bl/6J* mice with AIPD was similar to that reported for human psoriasis. By contrast, transcriptomic signatures in *BALB/cJ*, *129X1/SvJ*, *DBA*, and *MOLF* mice more closely resembled other human inflammatory skin conditions such as wounding, acne, and infections [11].

Forward genetics is an important method that features a combined evaluation of phenotypic variation and the genomic architecture to identify genetic polymorphisms associated with a given trait [12,13]. In this study, we used a forward genetics approach to identify polymorphisms associated with the clinical severity of AIPD in 13 inbred mouse strains. Our goal was to identify pathways promoting AIPD that might also elucidate the molecular pathogenesis of human plaque psoriasis. Using this approach, we identified several critical single nucleotide polymorphisms (SNPs) in *Itga11* that were associated with disease severity. Additional experiments highlighted the functional significance of *Itga11* and its role in promoting psoriasiform skin inflammation.

Materials and methods

Mice

All mouse experiments were approved by the animal ethics committee of the state of Schleswig-Holstein [AZ 5(55-5/14) and AZ 5(110-8/13)]; details about the strains used can be found in Supplementary materials and methods.

The AIPD mouse model

The AIPD mouse model was used as described previously [11], and all mice were scored daily with the modified Psoriasis Area and Severity Index (PASI) as previously described [14]. For more details see Supplementary materials and methods.

Histopathology and immunofluorescence

Formalin-fixed, paraffin-embedded skin sections were stained with H&E or probed with antibodies that targeted Ki-67 (BioLegend, San Diego, CA, USA), the macrophage/dendritic cells marker, F4/80 (AbD Serotec, Puchheim, Germany), the endothelial cell marker, CD31, and the T-cell marker, CD3 (BioLegend) [15]. For quantification of TRMs, frozen skin samples were stained with anti-CD3 (Becton Dickinson GmbH, Heidelberg, Germany) and anti-CD103 (R&D Systems, Minneapolis, MN, USA). Expression of vimentin was detected using the manufacturer's protocol with slight modifications. For more details see Supplementary materials and methods.

Haplotype analysis

Efficient Mixed-Model Association eXpedited (EMMAX) [16] and Haploview software [17] analysis from all available mouse strains was performed as described in Supplementary materials and methods.

RNA sequencing (RNA-seq)

Total RNA of WT and *Itga11*$^{-/-}$ KO littermates was extracted from back skin specimens with (n = 8/group) or without (n = 5/group) 4 days of AIPD. Sequencing was performed using Illumina NextSeq in high-output mode. For more details concerning the analysis workflow see Supplementary materials (Illumina Inc., San Diego, CA, USA). Sequencing data were submitted to the SRA database. https://www.ncbi.nlm.nih.gov/bioproject/PRJNA869122.

Deconvolution of RNA sequencing data

Deconvolution of bulk RNA sequencing (RNA-seq) data derived from our analysis of AIPD and healthy mouse skin was performed using publicly available single-cell RNA-seq (scRNA-seq) datasets from the U.S. National Center for Biotechnology Information (NCBI) sequence read archive (SRA) database available at accession numbers SRP 268188 [18] and

GSE129218 [19]. More details are presented in Supplementary materials and methods.

Statistics

All data are presented as mean ± standard error of the mean (SEM). Clinical scores were compared by two-way ANOVA with the Bonferroni multiple-comparisons test. Cutaneous cell infiltrations and clinical AUC data were analyzed using the Mann–Whitney U test or Kruskal–Wallis test with Dunn's *post hoc* test when more than two groups were compared. p values less than 0.05 were considered statistically significant throughout the study.

Results

High variability of clinical AIPD in different inbred mouse strains

We evaluated the severity and progression of AIPD in 13 different inbred mouse strains (Figure 1A–E and supplementary material, Figure S1). As anticipated, the PASI scores differed substantially between the strains. *NZO/HlLtJ* mice treated with Aldara® cream developed minimal disease, as indicated by a cumulative PASI score of 14.7 ± 1.23 (days 0–6) (Figure 1B). Similarly, *FVB/NJ* (cumulative PASI score, 17.0 ± 0.83) and *NOD/ShiltJ* (cumulative PASI score, 21.9 ± 1.08) mice also responded to the repetitive administration of Aldara® cream with less severe disease than was observed in *C57BL/6J* mice (cumulative PASI score, 30.1 ± 1.29). All components of the cumulative PASI score (erythema, infiltration, and desquamation) were affected equally in the aforementioned strains (Figure 1C–E). By contrast, *CAST/EiJ* mice (cumulative PASI score, 41.0 ± 2.92) were highly responsive to Aldara® cream and developed more severe psoriasiform dermatitis than was observed in any of the other mouse strains (Figure 1A–E, supplementary material, Figure S1 and Table S1). Notably, four of the six *CAST/EiJ* mice succumbed to this regimen within 6 days of the initial treatment due to weight loss and a bad general condition.

The differences in clinical severity correlated directly with differences in the critical histopathological features of psoriasiform dermatitis, specifically with epidermal thickness and dermal infiltration (Figure 2A–D). We compared skin sections from *CAST/EiJ*, *C57BL/6J*, and *NZO/HlLtJ* mice treated with Aldara® cream as representative of severe, intermediate, and mild manifestations of this disease (Figure 2A–C). The epithelial thickness and infiltration scores correlated directly with the aforementioned clinical signs of AIPD. Consistent with these findings, the proliferation marker Ki-67 was detected in the dermis and epidermis of *C57BL/6J* mice and was even more prominent in the skin of *CAST/EiJ* mice. No expression of Ki-67 was detected in the skin of *NZO/HlLtJ* mice (Figure 2D).

Identification of susceptibility loci for AIPD using a forward genetics approach

We used a forward genetics approach to identify associations between specific genes and the severity of AIPD using the average cumulative PASI score of each strain as the phenotypic parameter. Association analysis was then performed using EMMAX, which is a statistical test used for large-scale human or model organism association mapping that takes sample structure into account. We then performed a haplotype analysis by Haploview [17] to identify haplotype blocks that were significantly associated with the corresponding alleles. After permutation, the cutoff for the p value was set to 0.005. Using these methods, we identified several SNPs that were associated with AIPD (Table 1). The haplotype block contained 13 genes, including *Nckap5*, *Dcdc5*, *Caln1*, *Wbscr17*, *Auts2*, *Clec2f*, *Mctp2*, *Fem1b*, *Actn1*, *Adam21*, *Ttc9*, *Coro2b*, and *Itga11*. The most significant SNPs were rs30473931 and rs33676670 ($p = 0.001$), which are both located within intronic regions of the *Itga11* gene.

Itga11$^{-/-}$ mice are partially protected from developing AIPD

To examine the pathological significance of *Itga11* and its role in promoting the clinical findings associated with AIPD, we compared the responses of *Itga11*$^{-/-}$ mice and their WT littermates. While both WT and gene-deleted mice developed AIPD in response to the topical application of Aldara® cream, clinical severity was significantly reduced in the *Itga11*$^{-/-}$ strain (Figure 3A–E). The differences between these strains were apparent as early as day 1 and persisted through day 4. These differences were observed in all components of the PASI score (i.e., erythema, infiltration, and desquamation; Figure 3A–E). We also measured ear swelling for quantitative documentation of the severity of skin inflammation as previously described [20]. Ear swelling observed in response to the administration of Aldara® cream was also significantly attenuated in *Itga11*$^{-/-}$ mice (Figure 3F).

At the histopathological level, epidermal thickness and dermal leukocyte infiltration were significantly reduced in *Itga11*$^{-/-}$ mice compared to the WT (Figure 4A,B). Consistent with this finding, significantly fewer cells in the epidermis of *Itga11*$^{-/-}$ mice expressed Ki-67 compared to their WT littermates (Figure 4B). To characterize the histopathological differences between these mouse strains in greater detail, we determined the numbers of endothelial (CD31$^+$) cells, macrophages/dendritic (F4/80$^+$) cells (macrophages/DCs), and T (CD3$^+$) cells in representative skin sections (Figure 4B). All three cell populations have been identified as important drivers of AIPD and psoriasis, with increased numbers detected in psoriasiform and psoriatic skin [9,15,21,22]. While the numbers of dermal CD3$^+$ T cells and F4/80$^+$ macrophages/DCs were significantly lower in skin specimens from *Itga11*$^{-/-}$ mice at the final time point (day 4), we detected no differences in the

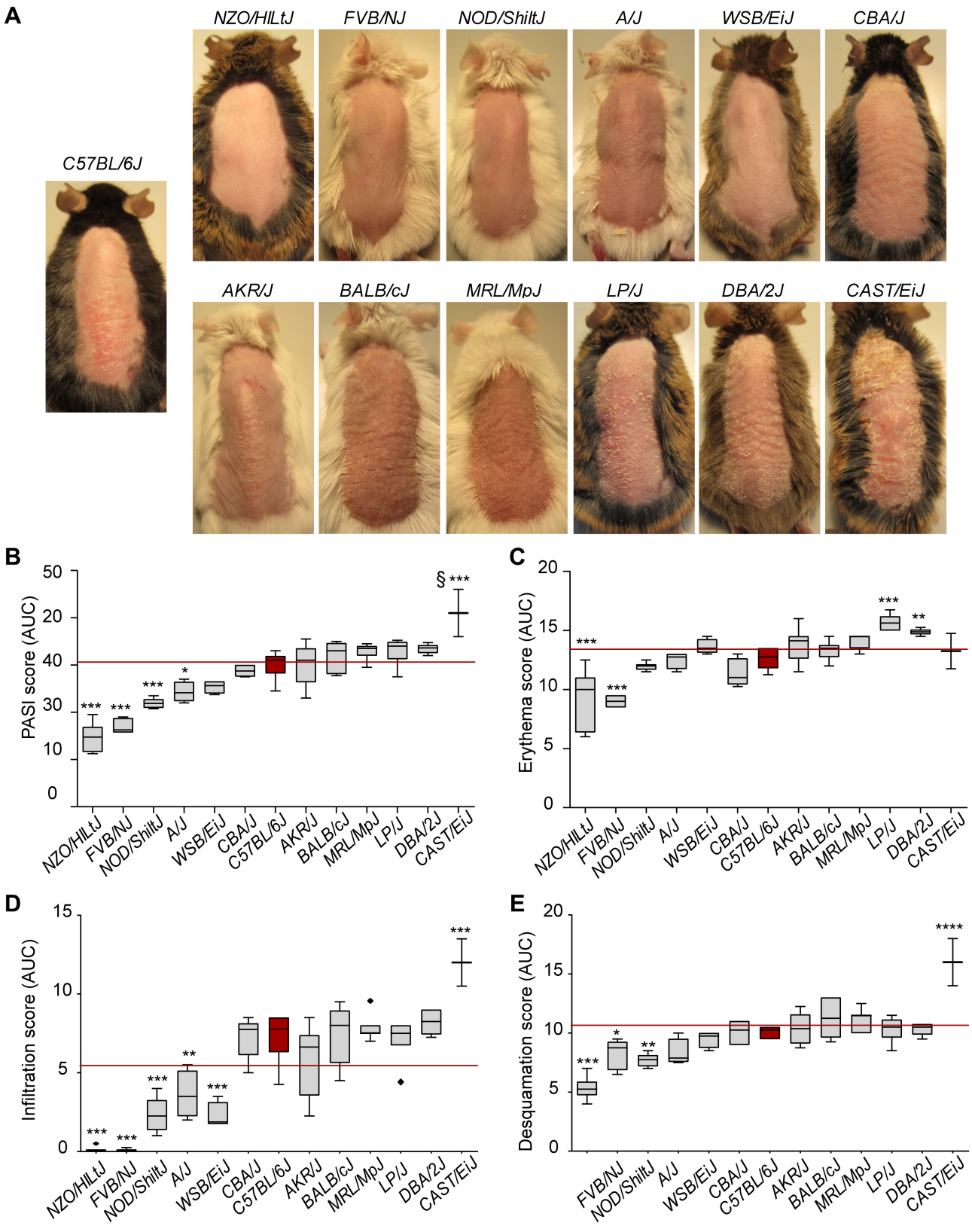

Figure 1. Clinical manifestations of AIPD are strain-dependent. AIPD was induced by topical administration of Aldara® cream to the dorsal skin of 13 different strains of inbred mice. Clinical disease severity was monitored daily for 6 days. (A) Representative images were obtained on day 6. Except for the reference *C57BL/6J* mouse strain, the images shown are presented in order from the lowest (upper left) to the highest (lower right) degree of disease severity. Tukey box-and-whisker plots of the areas under the curve (AUCs) document (B) the cumulative PASI scores and their individual subcomponents, including (C) erythema, (D) infiltration, and (E) desquamation over time; $n = 6$–8 mice per group. The horizontal red line shown in all plots represents the mean disease activity of all mouse strains included in this study. Disease severity in each strain was compared with the responses of the reference *C57BL/6J* strain (red box) using Kruskal–Wallis with Dunn's *post hoc* test; $^{*}p < 0.05$; $^{**}p < 0.01$; $^{***}p < 0.001$; §only mice that survived until the end of the experiment were included in the analysis.

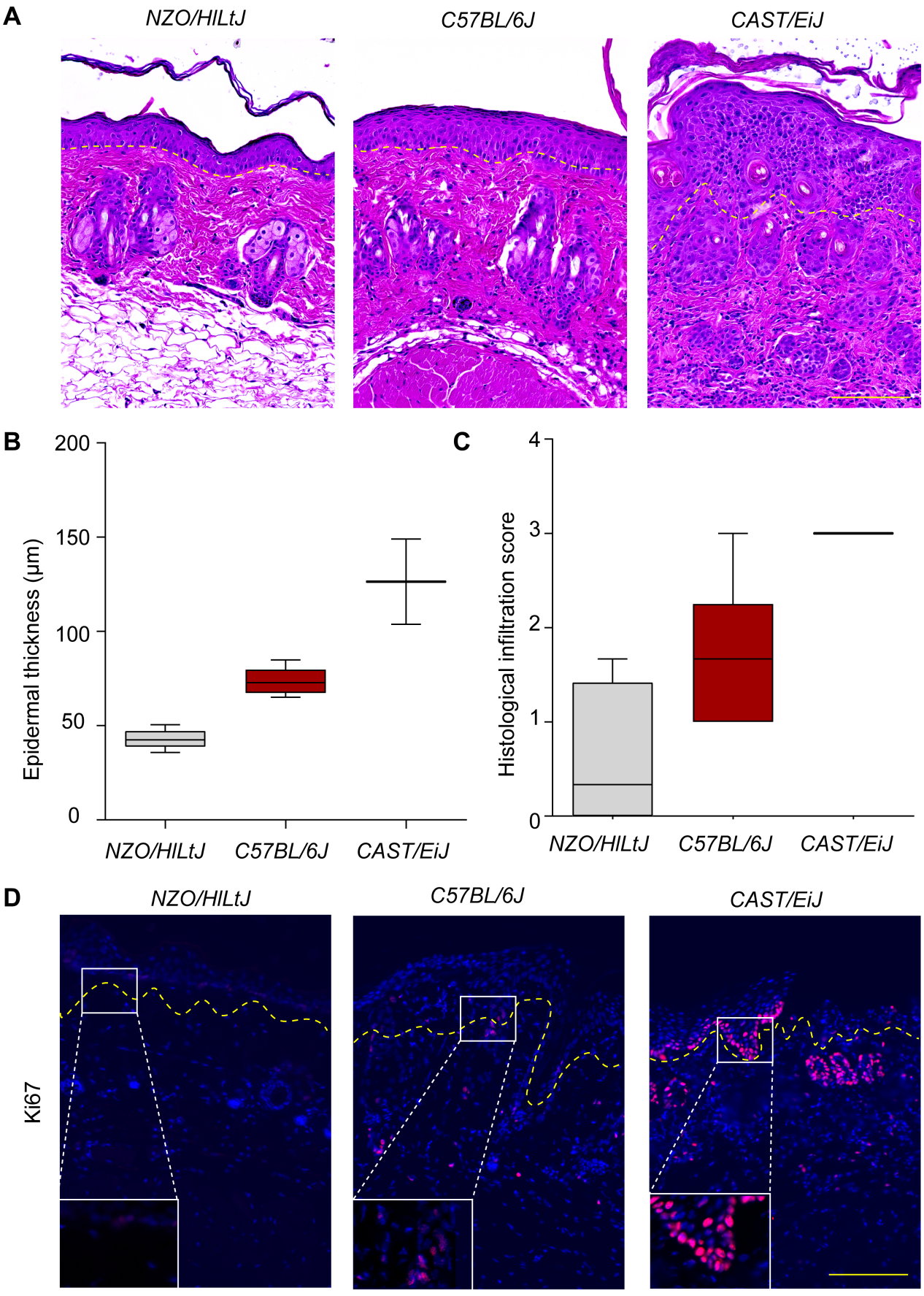

Figure 2 Legend on next page.

Table 1. A forward genetics approach identifies genes associated with AIPD. Genes associated with AIPD were identified by performing an association analysis using EMMAX. This was followed by Haploview, which was used to identify significantly associated haplotype blocks that included these alleles. After permutation, the cutoff for the *p* value was set to 0.005. The shaded grey lines indicate the *Itga11* SNPs.

CHR No.	SNP	Position on chromosome (bp)	*p* value	rsID	Gene
1	JAX00265501	124,891,086	0.00217	rs33381007	
1	JAX00265936	126,619,319	0.00217	rs33435190	*Nckap5*
1	JAX00265954	126,652,333	0.00217	rs33430705	*Nckap5*
2	JAX00098266	106,072,958	0.00217	rs27443160	*Dcdc5*
2	JAX00217654	106,074,005	0.00217	rs49058488	*Dcdc5*
5	JAX00597140	129,470,243	0.00217	rs37174132	
5	JAX00135761	130,819,242	0.00217	rs36983254	*Caln1*
5	JAX00135792	131,238,187	0.00217	rs36766036	*Wbscr17*
5	JAX00597593	131,319,140	0.00217	rs37880920	*Auts2*
5	JAX00135798	131,319,772	0.00217	rs36294244	*Auts2*
5	JAX00135839	131,859,049	0.00217	rs49334132	*Auts2*
6	JAX00625864	129,002,976	0.00217	rs49646778	*Clec2f*
6	JAX00146677	129,013,712	0.00217	rs48729719	*Clec2f*
7	JAX00643017	71,816,109	0.00217	rs38846554	
7	JAX00152764	72,221,145	0.00217	rs49313119	*Mctp2*
7	JAX00152770	72,309,762	0.00217	rs47351867	*Mctp2*
9	**JAX00172036**	**62,748,616**	**0.00125**	**rs30473931**	***Itga11***
9	**JAX00696238**	**62,765,722**	**0.00125**	**rs33676670**	***Itga11***
9	JAX00172041	62,813,075	0.00125	rs29586321	*Fem1b*
12	JAX00339411	80,163,406	0.00217	rs32634894	*Actn1*
12	JAX00339474	80,446,905	0.00217	rs32637849	*Actn1*
12	JAX00038301	81,556,920	0.00217	rs48366978	*Adam21*
12	JAX00339667	81,639,654	0.00217	rs46775824	*Ttc9*
12	JAX00339673	81,645,465	0.00217	rs47429428	*Ttc9*

number of $CD31^+$ endothelial cells (Figure 4B). A more in-depth investigation of the function of T cells in AIPD revealed that the site-specific disease memory has been linked to $CD3^+CD103^+$ tissue-resident memory T (TRM) cells. Importantly, the number of TRM cells identified in the skin remains elevated in mice with resolved AIPD disease. These findings suggest that a stable resting population of epidermal TRM cells develops in resolved psoriasis, which may contribute to psoriatic recurrence [23]. Thus, we aimed to investigate the role played by *Itga11* expression with respect to this cell type in AIPD. Of note, the deletion of *Itga11* almost completely prevented the increase of TRM cells in inflamed skin in AIPD (Figure 4C). Taken together, these findings reveal an overall reduction in skin inflammation in Aldara® cream-treated $Itga11^{-/-}$ mice.

Single-cell RNA-seq identifies fibroblasts as the predominant cellular source of *Itga11* in the skin of mice with AIPD

To identify the cellular source of *Itga11* mRNA in the skin of mice with AIPD, we used publicly available scRNA-seq data generated from the dorsal skin of WT *C57BL/6J* mice treated with a daily topical dose of 62.5 mg Aldara® cream [18]. Using a Seurat workflow, we identified 19 distinct clusters in the skin of *C57BL/6J* mice with AIPD. These clusters represent immune and nonimmune cell populations, including macrophages (clusters 0–5 and 11–12), neutrophils (cluster 6), T cells (cluster 7), adipocytes (cluster 8), myocytes (cluster 9), fibroblasts (cluster 10), keratinocytes (cluster 13), Langerhans cells (cluster 14), polarized epidermal cells (cluster 15), endothelial cells (cluster 16), B cells (cluster 17), and basophils (cluster 18) (Figure 5A). We annotated the individual clusters by determining the expression of canonical markers typically used in the literature for each cell population and by examining the predominant differentially regulated transcripts (supplementary material, Figure S2 and Table S2). Once we had defined the cellular architecture of the skin of *C57BL/6J* mice with AIPD, we determined that fibroblasts and, to a much lesser extent, macrophages and adipocytes expressed *Itga11* (Figure 5B,C). To further delineate the cellular source of *Itga11* mRNA in the skin of mice at homeostasis, we again performed deconvolution workflow using publicly available scRNA-seq data collected from dorsal skin samples of untreated WT

Figure 2. Measurements of epidermal thickness and leukocyte infiltration correspond directly to the strain-dependent clinical severity of AIPD. Tissue histopathology of skin specimens collected on day 6 from *NZO/HlLtJ* (mild disease), *C57BL/6J* (moderate disease), and *CAST/EiJ* mice (severe disease) was examined. (A) Representative images of skin specimens stained with H&E. Tukey box-and-whiskers plots of (B) the epidermal thickness and (C) semiquantitative assessments of leukocyte infiltration ($n = 2$–6 mice per group). (D) Representative images of skin tissue probed with antibodies that target the proliferation marker, Ki-67 (red). The dotted yellow lines in both (A) and (D) mark the dermal–epidermal junction. The insets in (D) document the expression of Ki-67 in the lowermost sections of the epidermis at a twofold higher magnification. Scale bar, 150 μm. Dotted line: dermal–epidermal junction.

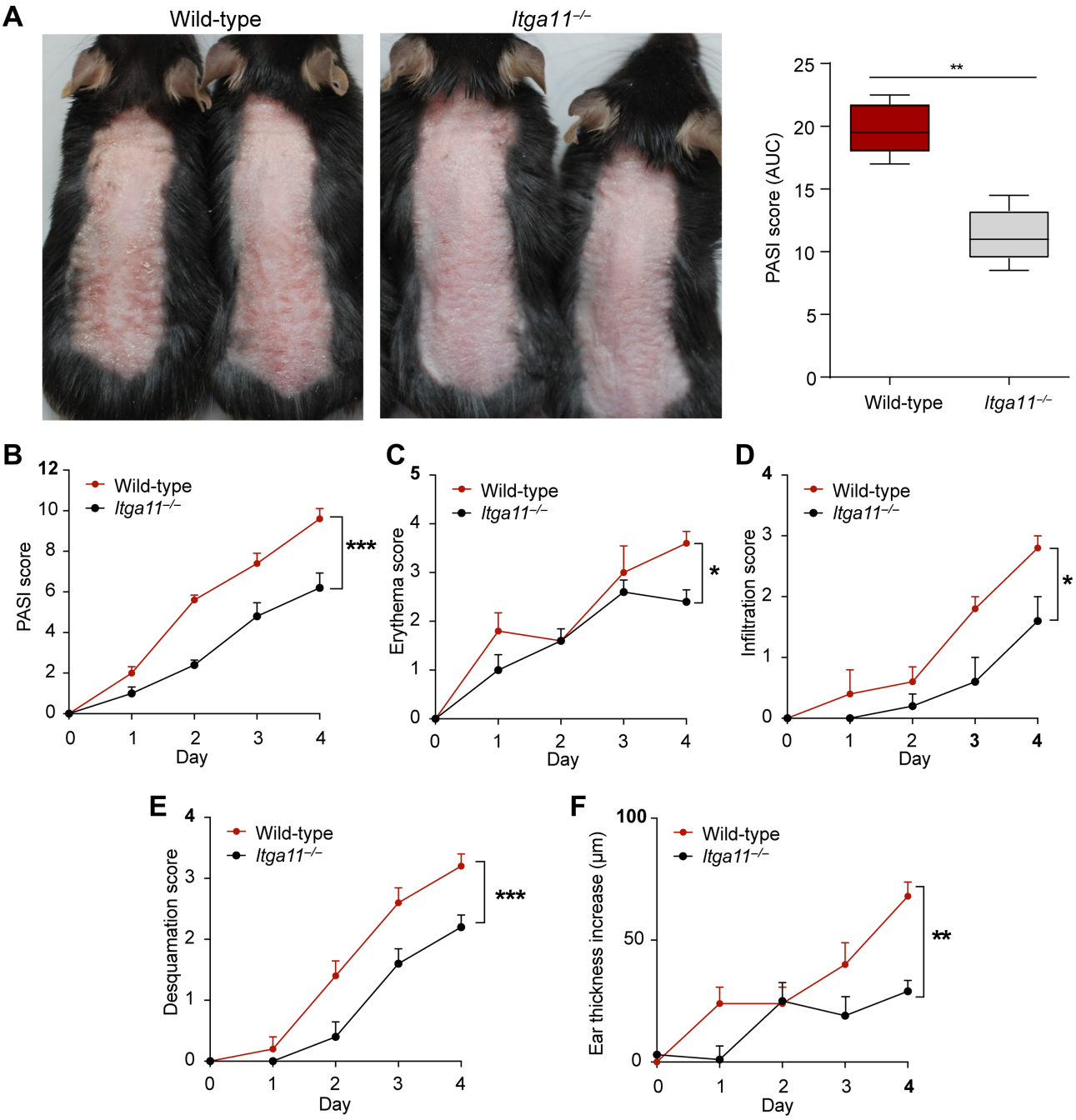

Figure 3. *Itga11*$^{-/-}$ mice are partially protected from AIPD. (A) Representative images and cumulative PASI scores of *Itga11*$^{-/-}$ mice and their WT littermates that were treated daily with Aldara® cream for a maximum of 4 days. (B) Cumulative PASI scores and their subcomponents, including (C) erythema, (D) infiltration, and (E) desquamation, are shown. (F) Ear swelling in response to local administration of Aldara® cream. All results are presented as the mean ± standard error of the mean (SEM). Data were analyzed by two-way ANOVA and Šidák's *post hoc* test ($n = 5$ mice per group). A representative of three experiments is presented; *$p < 0.05$; **$p < 0.01$; ***$p < 0.001$.

C57BL/6J mice [19]. Our findings clearly identified fibroblasts are the major cell type expressing *Itga11* (supplementary material, Figures S2–S4 and Table S3).

Itga11 deficiency alters cutaneous gene expression and the abundance of fibroblasts in the skin of mice with AIPD

To determine the impact of *Itga11* deficiency on cutaneous gene expression, we profiled and compared the skin transcriptomes of untreated and Aldara® cream-treated WT and *Itga11*$^{-/-}$ on day 4 using bulk RNA-seq. While the transcriptomes of untreated WT and *Itga11*$^{-/-}$ mice did not differ significantly from one another (Figure 6A), treatment with Aldara® cream resulted in profound and distinct changes in gene expression in both WT and *Itga11*$^{-/-}$ mice. Specifically, treatment with Aldara® cream resulted in the differential expression of 686 genes in WT versus *Itga11*$^{-/-}$ mice (Figure 6A–C).

To identify pathways that may contribute to the attenuation of AIPD in *Itga11*$^{-/-}$ mice, we performed Gene Set Enrichment Analysis (GSEA) of the differentially

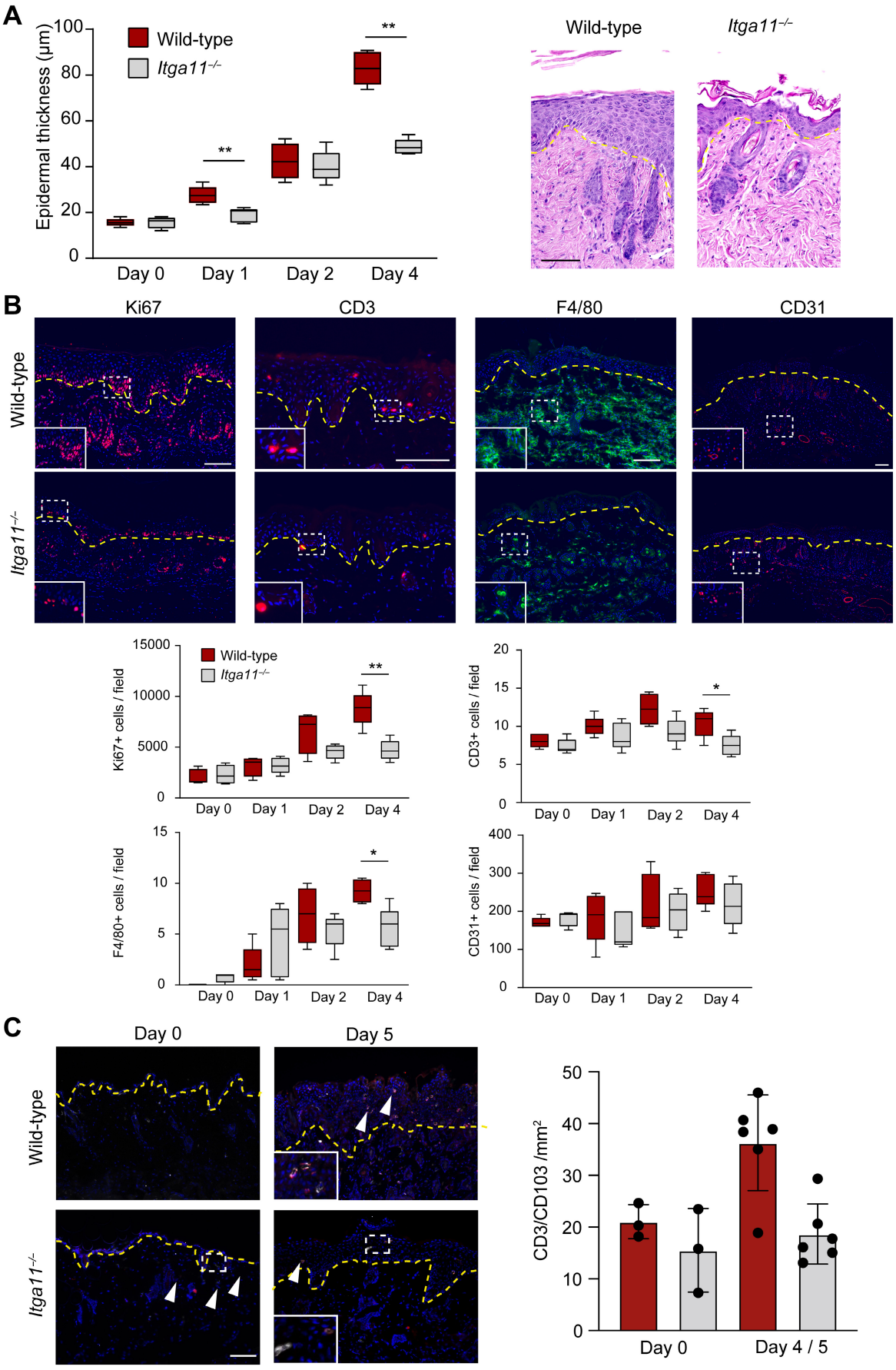

Figure 4 Legend on next page.

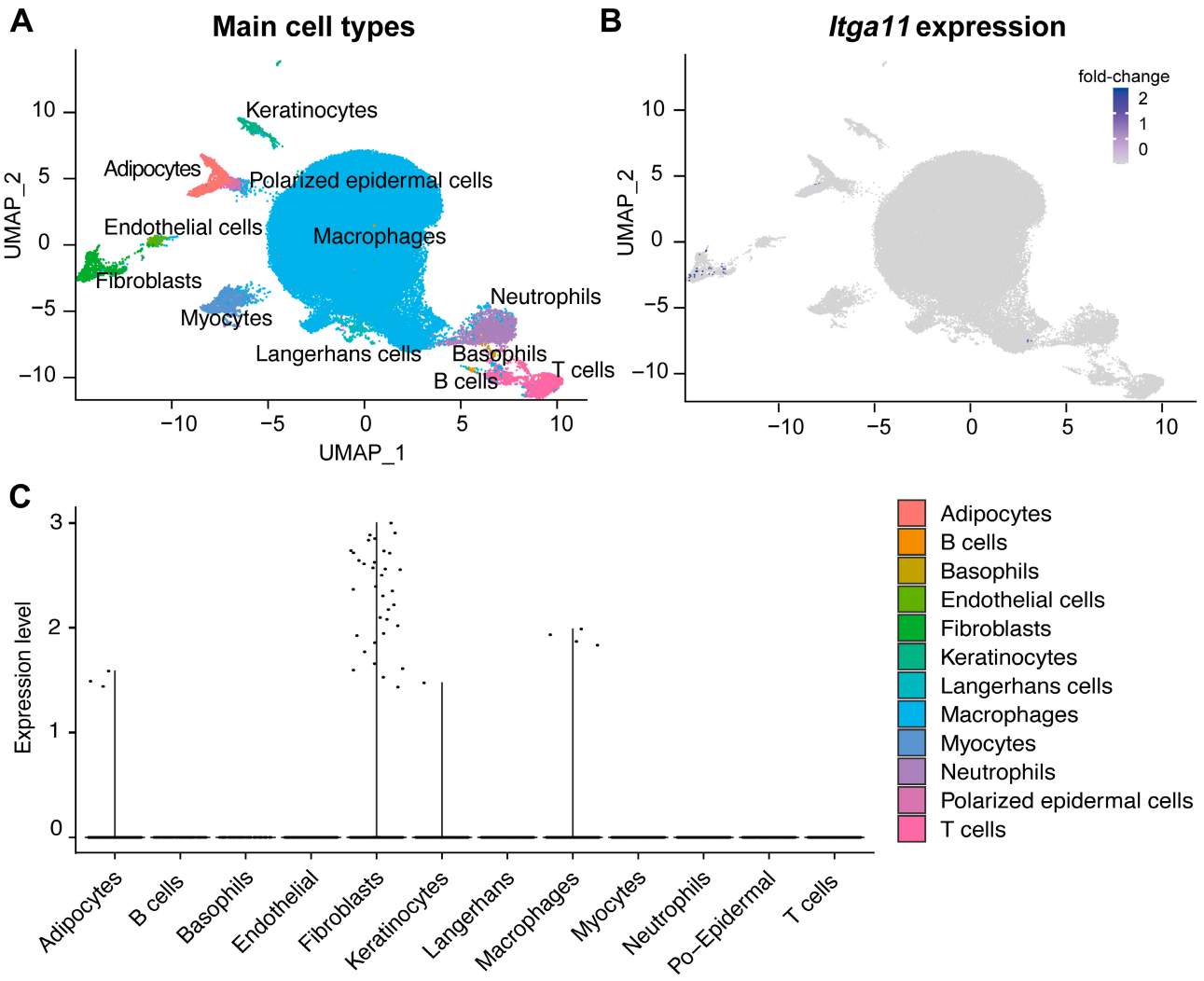

Figure 5. *Itga11* is expressed predominantly by fibroblasts in skin specimens from WT mice with AIPD skin. (A) Annotation of scRNA-seq data from skin tissue of WT *C57BL/6J* mice with AIPD. (B) Expression of mRNA transcripts encoding *Itga11* in scRNA-seq data from different cell clusters. (C) Violin plots documenting the expression of *Itga11* across the different clusters as determined by scRNA-seq. Po-Epidermal = polarized epidermal cells.

expressed genes using *Webgestalt* [24]. Using this method, we identified gene enrichment in 10 and gene downregulation in six known reactome pathways (Figure 6D, supplementary material, Table S4). We have provided details for the similar transcriptomes of WT and *Itga11*$^{-/-}$ mice under steady-state conditions as well as the changes and intergroup differences that develop in response to AIPD for three selected pathways, including *extracellular matrix (ECM) organization*, *immune system*, and *metabolism of lipids* (Figure 6E–G). Induction of AIPD in the WT mice resulted in a marked increase in gene expression associated with ECM organization and immune system pathways in the skin; these changes were not detected in the skin of Aldara® cream-treated *Itga11*$^{-/-}$ mice (Figure 6E,F). By contrast, gene expression associated

Figure 4. Key histological features of AIPD are less pronounced in *Itga11*-deficient mice. (A and B) Skin biopsies from both *Itga11*$^{-/-}$ and WT mice with AIPD were collected on days 0 (untreated), 1, 2, and 4. (A) Progression of the epidermal thickness (µm) in WT and *Itga11*$^{-/-}$ mice with AIPD (left panel) are as shown. Representative H&E-stained skin tissue specimens prepared from mice on day 4 (right panel). (B) Representative immunofluorescence/immunohistochemically stained skin specimens from *Itga11*$^{-/-}$ and WT mice and quantitative analysis of the expression of Ki-67 (red), CD3 (red), F4/80 (green), and CD31 (red) on day 4 of treatment with Aldara® cream. (C) Skin biopsies were obtained from both WT and *Itga11*$^{-/-}$ mice with AIPD on days 0 (untreated), 4, or 5. Quantification of TRM-positive cells in skin tissue from WT and *Itga11*$^{-/-}$ mice. Representative immunofluorescence staining for CD3 (AF680-labeled, white), CD103 (PE-labeled, red), and DAPI (blue) in murine skin tissue on days 0 and combined days 4 and 5 of the AIPD protocol. (A and B) Quantitative results are presented in Tukey box-and-whiskers plots (n = 4–5 mice per group). (C) Results are presented as scatter plots with median ± interquartile range (n = 3–6 mice per group). (A–C) Results were analyzed using Kruskal–Wallis and Dunn's *post hoc* tests (comparison by day); *p < 0.05; **p < 0.01. Scale bars, 150 µm. Dotted line: dermal–epidermal junction.

with the metabolism of lipids pathways was diminished in the skin of AIPD versus untreated WT mice, while gene expression associated with this pathway increased in AIPD versus untreated *Itga11*$^{-/-}$ counterparts (Figure 6G).

We then used the ENIGMA algorithm [25] to deconvolute bulk RNA-seq data into cell type-specific expression matrices. We used both the bulk RNA-seq and scRNA-seq data to characterize changes in the

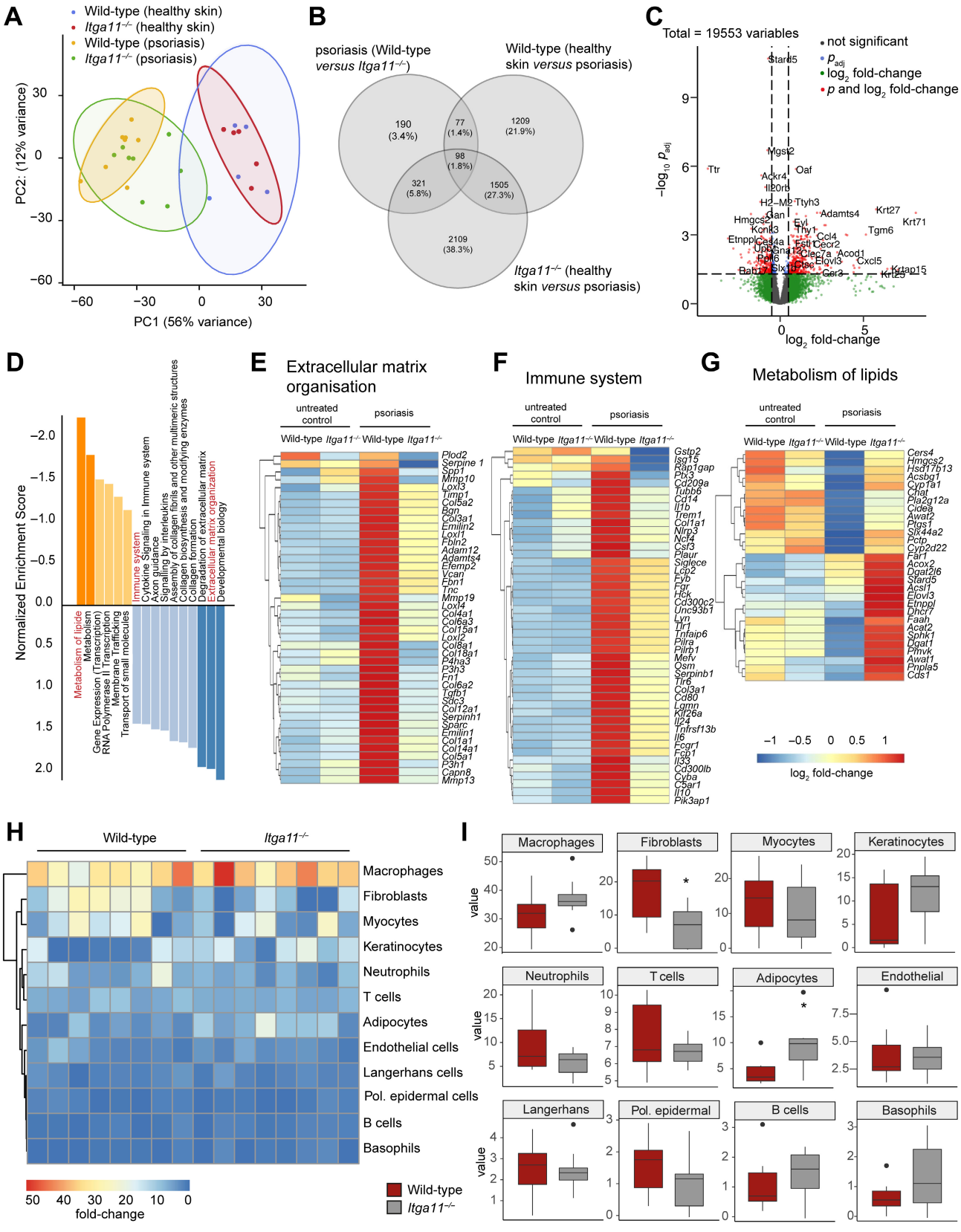

Figure 6 Legend on next page.

cellular composition of skin from WT and *Itga11*$^{-/-}$ mice with AIPD. Consistent with the significant changes in the ECM organization pathway and with the cellular expression pattern of *Itga11* in AIPD skin, we detected differences in the relative abundance (the evenness of distribution of individuals in the community) of fibroblasts and adipocytes when comparing WT and *Itga11*$^{-/-}$ mice. The results of this analysis predicted a significant reduction in the proportion of fibroblasts (relative abundance: WT, 17.4; *Itga11*$^{-/-}$, 7.0; $p = 0.01$) and a significant increase in the proportion of adipocytes (relative abundance: WT, 4.3; *Itga11*$^{-/-}$, 9.7; $p = 0.02$) in the skin of *Itga11*$^{-/-}$ mice (Figure 6H,I). To validate these observations, we probed skin sections of WT and *Itga11*$^{-/-}$ mice with AIPD with antibodies against the fibroblast marker vimentin (supplementary material, Figure S5). Consistent with the deconvolution analysis, our results revealed a significant reduction in vimentin expression in the dermis of *Itga11*$^{-/-}$ mice with AIPD. By contrast, the findings focused on adipocytes could not be confirmed by H&E staining of skin samples from mice with AIPD. Among the reasons for this discrepancy, the interindividual variance of fat distribution is very high in the dorsal skin of WT and *Itga11*$^{-/-}$ mice in our experiments, potentially because we included both male and female mice of different ages (supplementary material, Figure S6). Consistent with our RNA-seq data, our findings revealed no changes in the proportion of each cell type under homeostatic conditions (supplementary material, Figures S5 and S6). Therefore, we conclude that fibroblasts are the major source of *Itga11* in AIPD.

To confirm the RNA-seq data on the protein level, we included flow cytometric analysis of Itga11 expression on several critical cell types found in untreated skin and in response to AIPD, including fibroblasts, myocytes, T cells, and CD11b-positive leukocyte populations (i.e., granulocytes, macrophages, and dendritic cells). Our results revealed that fibroblasts are the major source of Itga11 (supplementary material, Figure S7), but some expression was also noted in myocytes and CD11b-positive cells (probably macrophages) in flow cytometry. Interestingly, increased expression of Itga11 was limited to fibroblasts in skin tissue from AIPD mice compared to untreated controls.

Discussion

In this study, we used a forward genetics approach to identify candidate loci that may contribute to the development of AIPD. Based on our clinical evaluation of 13 different mouse strains, we identified several SNPs that were associated with AIPD. The most significant genes within the haplotype block were located in the intronic regions of the *Itga11* gene. Interestingly, *Coro2b*, which encodes Coronin-2b, a regulator of actin dynamics, and *Fem1b*, which encodes the death receptor-associated ankyrin repeat protein FEM1b with characterized roles in mediating cell stress [26–29], are adjacent to *Itga11* on mouse chromosome 9. Notably, rs29586321, which is a SNP located in the 5'UTR of *Fem1b*, was also among the SNPs that were significantly associated with AIPD. Hence, although our present analysis revealed a role for *Itga11* as a central regulator of AIPD, other nearby genes may also be considered potential candidates.

The integrin α11 subunit dimerizes with the integrin β1 subunit to form the integrin α11β1 heterodimer. Integrin α11β1 is a collagen receptor that mediates adhesion between cells and the extracellular matrix [30,31]. The integrin α11 subunit is expressed by mesenchymal stem cells and subsets of fibroblasts and is detected at high levels in cardiac and skeletal muscle tissue, tendons, and perichondrial cells [31,32]. Accordingly, results from previous studies revealed that the integrin α11 subunit played an essential role in the maintenance of the skeletal bone mass and periodontal ligament-driven tooth eruption [32,33].

The role of *Itga11* in skin inflammation remains largely understudied. During skin wound healing, dermal fibroblasts lacking *Itga11* show defects in collagen remodeling and are unable to efficiently convert to myofibroblasts, resulting in scar tissue with compromised tensile strength. The clinical symptoms in mouse models can vary considerably in a broad range from isolated small areas to the involvement of the entire integument [34,35]. However, to our knowledge, to this day, no studies have highlighted the role of *Itga11* in psoriasis.

In this study, we underscore the role of *Itga11* as a modulator of psoriasiform dermatitis in the AIPD mouse model. Our transcriptomic analysis revealed that *Itga11*

Figure 6. The skin transcriptomes of WT and *Itga11*-deficient mice reveal differential gene expression only after induction of inflammation. Skin transcriptomes from Aldara® cream-treated or untreated WT and *Itga11*$^{-/-}$ mice were profiled by RNA-seq. (A) Principal component analysis (PCA) of transcriptomes from Aldara®-treated ($n = 8$ per group) and control-treated mice ($n = 5$ per group) document distinct expression patterns in untreated versus inflamed skin. (B) Venn diagram summarizes number of genes that were differentially regulated in skin transcriptomes of untreated versus Aldara® cream-treated WT and *Itga11*$^{-/-}$ mice. (C) Differentially regulated genes in skin specimens from *Itga11*$^{-/-}$ mice that were treated with Aldara® or left untreated are presented in a volcano plot. Genes highlighted in red were selected by $\log_2$ fold-change (FC), with adjusted p values. The default cutoff for $\log_2$FC was >2. (D) Results of *Webgestalt* enrichment of reactome pathways. The bar chart sorts the results by enrichment ratio (GSEA). GSEA results that are positively enriched are shown in blue, and those negatively enriched are shown in orange. Gene sets with a false discovery rate (FDR) < 0.05 are colored in a darker shade. Heatmaps (scaled by row) of differentially expressed genes associated with pathways are shown, including (E) ECM organization (size = 48; normalized enrichment score = 1.89; $p = 0.000e{+}0$; FDR = 2.146e-2), (F) immune system (size = 94; normalized enrichment score = 1.37; $p = 6.508e{-}2$; FDR = 2.461e-1), and (G) metabolism of lipids (size = 48; normalized enrichment score = −2.18; $p = 0.000e{+}0$; FDR = 2.157e-2). A heatmap (H) and box plot (I) are shown that represent the predicted proportions of the 12 major cell types for each bulk RNA-seq of dorsal skin samples from *Itga11*$^{-/-}$ mice and WT controls with AIPD (day 4). Po-Epidermal, polarized epidermal cells.

mRNA was constitutively expressed at relatively low levels in untreated skin and was upregulated during the progression of AIPD. Notably, *Itga11* deficiency had no impact on the cutaneous transcriptome under physiological conditions but resulted in major changes to gene expression in response to AIPD. These results suggest that integrin α11β1 does not play a significant role in maintaining skin homeostasis but contributes substantially to the modulation of skin inflammation.

Previous studies focused on integrin α11β1 in the skin revealed a role for this protein in the regulation of cutaneous wound healing, specifically the development of dermal fibrosis [34,35]. Nevertheless, the biological function of α11β1 in the regulation of tissue inflammation remains unknown. Our RNA-seq data demonstrated that *Itga11* deficiency had a major impact on the ECM organization pathway and affected the expression of genes encoding several matrix metallopeptidases (MMPs) and collagens in the skin. These findings are consistent with those presented in previous publications demonstrating the impact of the flightless I actin binding protein (Flii) in the pathogenesis of AIPD [36]. Interestingly, Flii is also secreted by fibroblasts and macrophages [37,38]. Furthermore, the actin cytoskeleton mediates a central mechanism that promotes the mechanical interactions between these cells and the surrounding ECM and neighboring cells [39]. Therefore, fibroblasts may be important contributors to AIPD via their capacity to build supporting structures in the ECM.

Our bulk RNA-seq data demonstrated both changes in the structure of the ECM and reduced activation of the immune system KEGG pathway in *Itga11*$^{-/-}$ mice compared to WT mice after AIPD induction. This immune system regulation can be due to a direct effect of the *Itga11* expression on leukocytes or a secondary effect resulting from alterations in the ECM. In line with that, previous data demonstrated the potential impact of ECM reorganization on leukocyte extravasation and interstitial migration in the skin. Leukocyte infiltration is a critical feature of AIPD [9,40] and is the result of a multistep process that begins with leukocyte extravasation from the blood and their migration across endothelial cells and into the skin [41]. Once within the skin, leukocytes migrate through the ECM to their site of action [42]. Considering the impact of integrin α11 subunit deficiency on the ECM, this condition might also have a major impact on the migration of leukocytes in the dermis. Specifically, inflammatory stimuli induce the release of MMPs and cytokines from resident fibroblasts that lead to the generation of bioactive ECM fragments; these fragments perpetuate inflammation by modulating leukocyte chemotaxis, activation, differentiation, and survival [42]. Specifically, our findings revealed that *Mmp10*, *Mmp13*, and *Mmp19* were differentially expressed in skin transcriptomes of WT and *Itga11*$^{-/-}$ with AIPD. Among these mediators, Beck *et al*. [43] found that MMP19 was essential for T-cell-mediated cutaneous immune responses. Similarly, MMP10 modulates leukocyte recruitment and activation in the lung [44]. This concept is further supported by reports that document the impact of collagen density on T-cell responses [45] and the contributions of the ECM to T-cell mobility [36]. These data are consistent with our findings of fewer CD3^{+} T cells and TRM cells in *Itga11*$^{-/-}$ mice compared to WT mice following AIPD induction. Because TRM cells likely contribute to site-specific disease memory in psoriasis and persist in resolved lesions [26], further elucidation of the impact of *Itga11* during the chronic phase of the disease warrants more investigation.

Integrin signaling can also modulate paracrine signaling from dermal fibroblasts. We have also reported that fewer fibroblasts are detected in skin samples from *Itga11*$^{-/-}$ mice. Thus, α11β1, as a collagen-binding receptor, may have an impact on leukocyte migration into the skin via its capacity to alter the properties of the ECM and paracrine signaling, resulting in a shift toward a more proinflammatory state in response to a pathophysiologic challenge. Further analysis is needed to clarify if *Itga11* contributes to inflammatory mononuclear cell infiltration or rather prevents the resolution of the inflammation by affecting actin remodeling and extracellular organization during AIPD. One limitation of this study is the fact that our investigation focused only on the impact of Itga11 on the acute phase of AIPD. We recognize that Itga11 may also affect the chronic phase, notably due to its impact on ECM organization. Future studies using chronic models of psoriasis [26] might be performed to address these issues. Further studies, including a direct comparison of fibroblasts derived from *Itga11*$^{-/-}$ and WT mice, will be needed for an in-depth understanding of the molecular mechanisms via which *Itga11* deficiency contributes to the observed inflammation-mediated disruption of the ECM.

In summary, we demonstrate that the pathophysiology of AIPD is regulated by *Itga11* and that *Itga11* promotes psoriasiform dermatitis. Interestingly, under physiological conditions, *Itga11* deficiency has no impact on global gene expression in the skin. As *Itga11*$^{-/-}$ mice do not show any noticeable skin phenotype under homeostatic conditions, other integrins likely compensate for the absence of Itga11. By contrast, marked differences emerge in response to AIPD-associated inflammation. These differences reflect the overall impact of *Itga11* on ECM organization and the subsequent inflammatory process. Collectively, our results suggest that the integrin α11 subunit may be an important therapeutic target for the treatment of psoriasiform skin conditions. Specifically, inhibition of gene expression and/or protein activity may serve to counteract skin inflammation while having little to no adverse impact on unaffected skin.

Acknowledgements

We thank Nathalie Guillen and Claudia Kauderer for excellent technical support. We thank Jun Liu and Chenxin Qie (both from the Jiangsu key lab of Drug Screening, China Pharmaceutical University, Nanjing,

PR China) for their help with the scRNA-seq data. The project was supported by the University of Lübeck and the Cluster of Excellence 'Precision Medicine in Inflammation Medicine' (DFG EXC 2167) and a Research Council of Norway Centre of excellence grant (ID 223250) and Norwegian Cancer Society grant (KF-223052). Open Access funding enabled and organized by Projekt DEAL.

Author contributions statement

CDS was responsible for conceptualization and methodology. KB, SB, NG, JP, J-PS, MB, SM, AH and SK performed investigations. KB, YG, AV, TS and MB curated the data. KB, RJL and CDS wrote the original draft manuscript. CDS acquired funding and managed the project. DG, SMI, RJL and CDS provided resources. KB and CDS provided supervision.

Data availability statement

Sequencing data were submitted to the Sequence Read Archive (SRA) database. https://www.ncbi.nlm.nih.gov/bioproject/PRJNA869122.

References

1. Parisi R, Iskandar IYK, Kontopantelis E, *et al*. National, regional, and worldwide epidemiology of psoriasis: systematic analysis and modelling study. *BMJ* 2020; **369:** m1590.
2. Tsoi LC, Stuart PE, Tian C, *et al*. Large scale meta-analysis characterizes genetic architecture for common psoriasis associated variants. *Nat Commun* 2017; **8:** 15382.
3. Papp K, Gordon K, Thaci D, *et al*. Phase 2 trial of selective tyrosine kinase 2 inhibition in psoriasis. *N Engl J Med* 2018; **379:** 1313–1321.
4. Reich K, Papp KA, Blauvelt A, *et al*. Tildrakizumab versus placebo or etanercept for chronic plaque psoriasis (reSURFACE 1 and reSURFACE 2): results from two randomised controlled, phase 3 trials. *Lancet* 2017; **390:** 276–288.
5. Schön MP. Animal models of psoriasis: a critical appraisal. *Exp Dermatol* 2008; **17:** 703–712.
6. Swindell WR, Johnston A, Carbajal S, *et al*. Genome-wide expression profiling of five mouse models identifies similarities and differences with human psoriasis. *PLoS One* 2011; **6:** e18266.
7. Walter A, Schäfer M, Cecconi V, *et al*. Aldara activates TLR7-independent immune defence. *Nat Commun* 2013; **4:** 1560.
8. Flutter B, Nestle FO. TLRs to cytokines: mechanistic insights from the imiquimod mouse model of psoriasis. *Eur J Immunol* 2013; **43:** 3138–3146.
9. van der Fits L, Mourits S, Voerman JS, *et al*. Imiquimod-induced psoriasis-like skin inflammation in mice is mediated via the IL-23/IL-17 axis. *J Immunol* 2009; **182:** 5836–5845.
10. Bezdek S, Hdnah A, Sezin T, *et al*. The genetic difference between C57Bl/6J and C57Bl/6N mice significantly impacts Aldara™-induced psoriasiform dermatitis. *Exp Dermatol* 2017; **26:** 349–351.
11. Swindell WR, Michaels KA, Sutter AJ, *et al*. Imiquimod has strain-dependent effects in mice and does not uniquely model human psoriasis. *Genome Med* 2017; **9:** 24.
12. Sadeghi H, Lockmann A, Hund AC, *et al*. Caspase-1-independent IL-1 release mediates blister formation in autoantibody-induced tissue injury through modulation of endothelial adhesion molecules. *J Immunol* 2015; **194:** 3656–3663.
13. Vorobyev A, Gupta Y, Sezin T, *et al*. Gene-diet interactions associated with complex trait variation in an advanced intercross outbred mouse line. *Nat Commun* 2019; **10:** 4097.
14. Sezin T, Kempen L, Meyne LM, *et al*. GPR15 is not critically involved in the regulation of murine psoriasiform dermatitis. *J Dermatol Sci* 2019; **94:** 196–204.
15. Bezdek S, Leng L, Busch H, *et al*. Macrophage migration inhibitory factor (MIF) drives murine psoriasiform dermatitis. *Front Immunol* 2018; **9:** 2262.
16. Kang HM, Sul JH, Service SK, *et al*. Variance component model to account for sample structure in genome-wide association studies. *Nat Genet* 2010; **42:** 348–354.
17. Barrett JC, Fry B, Maller J, *et al*. Haploview: analysis and visualization of LD and haplotype maps. *Bioinformatics* 2005; **21:** 263–265.
18. Qie C, Jiang J, Liu W, *et al*. Single-cell RNA-seq reveals the transcriptional landscape and heterogeneity of skin macrophages in Vsir$^{-/-}$ murine psoriasis. *Theranostics* 2020; **10:** 10483–10497.
19. Joost S, Annusver K, Jacob T, *et al*. The molecular anatomy of mouse skin during hair growth and rest. *Cell Stem Cell* 2020; **26:** 441–457.e7.
20. Wannick M, Bezdek S, Guillen N, *et al*. Oral administration of the selective GPR120/FFA4 agonist compound a is not effective in alleviating tissue inflammation in mouse models of prototypical autoimmune diseases. *Pharmacol Res Perspect* 2018; **6:** e00438.
21. Greb JE, Goldminz AM, Elder JT, *et al*. Psoriasis. *Nat Rev Dis Primers* 2016; **2:** 16082.
22. Chawla N, Kataria SP, Aggarwal K, *et al*. Significance of vascular endothelial growth factor and CD31 and morphometric analysis of microvessel density by CD31 receptor expression as an adjuvant tool in diagnosis of psoriatic lesions of skin. *Indian J Pathol Microbiol* 2017; **60:** 189–195.
23. Fenix K, Wijesundara DK, Cowin AJ, *et al*. Immunological memory in imiquimod-induced murine model of psoriasiform dermatitis. *Int J Mol Sci* 2020; **21:** 7228.
24. Liao Y, Wang J, Jaehnig EJ, *et al*. WebGestalt 2019: gene set analysis toolkit with revamped UIs and APIs. *Nucleic Acids Res* 2019; **47:** W199–W205.
25. Wang Z, Fong KD, Phan TT, *et al*. Increased transcriptional response to mechanical strain in keloid fibroblasts due to increased focal adhesion complex formation. *J Cell Physiol* 2006; **206:** 510–517.
26. Chen Y, Xu J, Zhang Y, *et al*. Coronin 2B regulates dendrite outgrowth by modulating actin dynamics. *FEBS Lett* 2020; **594:** 2975–2987.
27. Zhou Y, He L, Liu XD, *et al*. Integrated analysis of lncRNA and mRNA transcriptomes reveals new regulators of ubiquitination and the immune response in silica-induced pulmonary fibrosis. *Biomed Res Int* 2019; **2019:** 6305065.
28. Gandhi M, Goode BL. Coronin: the double-edged sword of actin dynamics. *Subcell Biochem* 2008; **48:** 72–87.
29. Manford AG, Mena EL, Shih KY, *et al*. Structural basis and regulation of the reductive stress response. *Cell* 2021; **184:** 5375–5390.e16.
30. Tiger CF, Fougerousse F, Grundström G, *et al*. alpha11beta1 integrin is a receptor for interstitial collagens involved in cell migration and collagen reorganization on mesenchymal nonmuscle cells. *Dev Biol* 2001; **237:** 116–129.
31. Koivunen J, Tu H, Kemppainen A, *et al*. Integrin α11β1 is a receptor for collagen XIII. *Cell Tissue Res* 2021; **383:** 1135–1153.
32. Popova SN, Barczyk M, Tiger CF, *et al*. Alpha11 beta1 integrin-dependent regulation of periodontal ligament function in the erupting mouse incisor. *Mol Cell Biol* 2007; **27:** 4306–4316.
33. Shen B, Vardy K, Hughes P, *et al*. Integrin alpha11 is an osteolectin receptor and is required for the maintenance of adult skeletal bone mass. *Elife* 2019; **8:** e42274.

34. Schulz JN, Zeltz C, Sørensen IW, *et al*. Reduced granulation tissue and wound strength in the absence of α11β1 integrin. *J Invest Dermatol* 2015; **135:** 1435–1444.
35. Schulz JN, Plomann M, Sengle G, *et al*. New developments on skin fibrosis – essential signals emanating from the extracellular matrix for the control of myofibroblasts. *Matrix Biol* 2018; **68–69:** 522–532.
36. Moreau JF, Pradeu T, Grignolio A, *et al*. The emerging role of ECM crosslinking in T cell mobility as a hallmark of immunosenescence in humans. *Ageing Res Rev* 2017; **35:** 322–335.
37. Franzén O, Gan LM, Björkegren JLM. PanglaoDB: a web server for exploration of mouse and human single-cell RNA sequencing data. *Database (Oxford)* 2019; **2019:** baz046.
38. Liao Y, Smyth GK, Shi W. featureCounts: an efficient general purpose program for assigning sequence reads to genomic features. *Bioinformatics* 2014; **30:** 923–930.
39. Love MI, Huber W, Anders S. Moderated estimation of fold change and dispersion for RNA-seq data with DESeq2. *Genome Biol* 2014; **15:** 550.
40. Terhorst D, Chelbi R, Wohn C, *et al*. Dynamics and transcriptomics of skin dendritic cells and macrophages in an imiquimod-induced, biphasic mouse model of psoriasis. *J Immunol* 2015; **195:** 4953–4961.
41. Schön MP, Ludwig RJ. Lymphocyte trafficking to inflamed skin–molecular mechanisms and implications for therapeutic target molecules. *Expert Opin Ther Targets* 2005; **9:** 225–243.
42. Sorokin L. The impact of the extracellular matrix on inflammation. *Nat Rev Immunol* 2010; **10:** 712–723.
43. Beck IM, Rückert R, Brandt K, *et al*. MMP19 is essential for T cell development and T cell-mediated cutaneous immune responses. *PLoS One* 2008; **3:** e2343.
44. Wight TN, Frevert CW, Debley JS, *et al*. Interplay of extracellular matrix and leukocytes in lung inflammation. *Cell Immunol* 2017; **312:** 1–14.
45. Kuczek DE, Larsen AMH, Thorseth ML, *et al*. Collagen density regulates the activity of tumor-infiltrating T cells. *J Immunother Cancer* 2019; **7:** 68.
46. Satija R, Farrell JA, Gennert D, *et al*. Spatial reconstruction of single-cell gene expression data. *Nat Biotechnol* 2015; **33:** 495–502.
47. Korsunsky I, Millard N, Fan J, *et al*. Fast, sensitive and accurate integration of single-cell data with harmony. *Nat Methods* 2019; **16:** 1289–1296.

References 46 and 47 are cited only in the supplementary material.

SUPPLEMENTARY MATERIAL ONLINE

Supplementary materials and methods

Figure S1. The clinical course of Aldara®-induced psoriasiform dermatitis (AIPD) is strain-dependent

Figure S2. Automatic clustering of scRNA-seq data from skin tissue

Figure S3. *Itga11* is predominantly expressed by fibroblasts in skin specimens from untreated WT mice

Figure S4. The skin transcriptomes of WT and *Itga11*-deficient mice reveal no differential cell distribution

Figure S5. Expression of vimentin in skin tissue from WT and *Itga11*$^{-/-}$ mice with AIPD

Figure S6. Histology of skin tissue from WT and *Itga1*$^{-/-}$ mice with AIPD

Figure S7. Expression of immunoreactive Itga11 in skin tissue from WT mice

Table S1. The clinical course of Aldara®-induced psoriasiform dermatitis (AIPD) is strain-dependent

Table S2. Cell type-specific marker genes used for cluster annotation of skin from mice with Aldara®-induced psoriasiform dermatitis (AIPD)

Table S3. Cell type-specific marker genes used for cluster annotation of untreated skin

Table S4. Kyoto Encyclopedia of Genes and Genomes (KEGG) pathways regulated by *Itga11* in AIPD